

IRAS03063+5735: A Bowshock Nebula Powered by an Early B Star

Henry A. Kobulnicky, Michael J. Lundquist, Anirban Bhattacharjee

Department of Physics & Astronomy

1000 E. University

University of Wyoming

Laramie, WY 82071, USA

Electronic Mail: chipk@uwyo.edu, mlundqui@uwyo.edu, abhattac@uwyo.edu

C. R. Kerton

Department of Physics and Astronomy

Iowa State University

Ames, IA 50011, USA

Electronic Mail: kerton@iastate.edu

ABSTRACT

Mid-infrared images from the *Spitzer Space Telescope* Galactic Legacy Infrared MidPlane Survey Extraordinaire program reveal that the infrared source IRAS 03063+5735 is a bowshock nebula produced by an early B star, 2MASS 03101044+5747035. We present new optical spectra of this star, classify it as a B1.5 V, and determine a probable association with a molecular cloud complex at $V_{LSR} = -38 - -42$ km s⁻¹ in the outer Galaxy near $\ell = 140.59^\circ$, $b = -0.250^\circ$. On the basis of spectroscopic parallax, we estimate a distance of 4.0 ± 1 kpc to both the bowshock nebula and the molecular complex. One plausible scenario is that this is a high-velocity runaway star impinging upon a molecular cloud. We identify the H II region and stellar cluster associated with IRAS 03064+5638 at a projected distance of 64 pc as one plausible birth site. The spectrophotometric distance and linkage to a molecular feature provides another piece of data helping to secure the ill-determined rotation curve in the outer Galaxy. As a by-product of spectral typing this star, we present empirical spectral diagnostic diagrams suitable for approximate spectral classification of O and B stars using He lines in the little-used yellow-red portion of the optical spectrum.

Subject headings: stars: early-type – stars: individual:2MASS 03101044+5747035
— infrared: ISM

1. Introduction

Short-lived massive stars typically lie within the OB associations in which they were born. However, a significant fraction (17%–50%) having high (30–200 km s^{−1}) space velocities wander far from such associations and are known as “runaways” (Blaauw 1961; Stone 1982; Conti et al. 1977; Gies & Bolton 1986). While many runaways are detected directly on the basis of large radial velocities or high proper motions, others are inferred by the presence of a tell-tale bowshock produced by their supersonic motion through the surrounding medium. van Buren & McCray (1988), van Buren et al. (1995), and Noriega-Crespo et al. (1997) used *Infrared Astronomical Satellite (IRAS)* images to locate arc-shaped bowshock features associated with high-velocity O stars. Bowshocks associated with high-velocity O stars have been detected more easily using the recent generation of mid-infrared surveys with higher angular resolution performed by the *Midcourse Space Experiment (MSX)* and the *Spitzer Space Telescope (SST)*. Recent studies of bowshocks around massive stars include Brown & Bomans (2005), Comerón & Pasquali (2007), Gvaramadze & Bomans (2008), and Povich et al. (2008). In Kobulnicky et al. (2010) we used the *SST* Cygnus-X Legacy Survey data to identify several probable runaway stars and their bowshocks in the vicinity of the Cygnus OB2 association while introducing a novel technique to exploit bowshock physics in order to estimate mass-loss rates from massive stars.

In this contribution we report the discovery that infrared source IRAS 03063+5735 is a bowshock nebula associated with an early B star in the outer Galaxy near $\ell = 140.59^\circ$, $b = -0.250^\circ$. Data from the *SST* Galactic Legacy Infrared MidPlane Survey Extraordinaire 360 (GLIMPSE 360) mid-infrared survey reveals the bowshock morphology for the first time. We use optical spectroscopy from the Wyoming Infrared Observatory (WIRO) 2.3 m telescope to determine a spectral type and radial velocity. These data, in turn, enable an estimate for the distance to the star and an associated molecular cloud complex.

2. Data

2.1. Discovery and Infrared Imaging Data

GLIMPSE 360 is a *SST* warm mission legacy program survey of the outer Galaxy in the [3.6] and [4.5] μm bandpasses (bands 1 & 2) of the Infrared Array Camera (IRAC Fazio et al.

2004). As part of a systematic study of “intermediate-mass” star-forming regions where stars up to $\sim B0$ are being formed, our team has been investigating IRAS sources having colors characteristic of soft UV radiation fields from early-to-mid B stars. IRAS 03063+5735 was initially selected as having *IRAS* colors indicating a such a soft radiation field similar to Galactic star forming regions hosting intermediate-mass stars (Kerton 2002; Arvidsson et al. 2010).¹ Our visual examination of IRAS 03063+5735 in GLIMPSE 360 images revealed a striking bilateral symmetric bowshock morphology at [3.6] and [4.5]. Figure 1 (right panel) shows a color representation of the nebula with the *SST* [3.6], [4.5], and *Wide-Field Infrared Survey Explorer* (*WISE*; Wright et al. 2010) band W3 [12.1] μm image in blue, green, and red, respectively. The nebula has a diameter of $\sim 2'$. A star, 2MASS 03101044+5747035 (hereafter Star A), lies near its center and along the axis of symmetry, making it the probable progenitor star. The left panel shows the 2MASS (The Two Micron All Sky Survey 2006) *J/H/K_s* image in blue/green/red, respectively. Note the presence of two infrared-bright rims in the mid-IR images. The first, with an apsis located $\sim 7''$ from Star A, is yellow-green in color, indicating relatively strong emission in the [4.5] (green) band. Diffuse emission in this band is typically dominated by shocked molecular hydrogen often seen in outflows from young stellar objects (Reach et al. 2006; Davis et al. 2007; Cyganowski et al. 2008), although the Brackett α line is also in this bandpass. The second, with apsis $\sim 27''$ from Star A, is relatively brighter in the [3.6] and [12.1] bands, giving it a reddish-white hue in Figure 1, but it is present at [4.5] as well. The [3.6] band contains broad polycyclic aromatic hydrocarbon (PAH) features while the [12.1] band contains both PAH features and a contribution from hot dust grains.

2.2. WIRO Optical Spectroscopy

We obtained optical longslit spectra of Star A at the WIRO 2.3 m telescope on the nights of 2011 October 23 & 27 using the 900 l/mm grating in first order over the wavelength range 4300 – 7300 Å. A total of seven 600-second exposures were obtained with a $2'' \times 150''$ slit in $\sim 2''$ seeing with an east-west slit orientation on 23 October and a north-south slit on 27 October. Spectra were wavelength calibrated using CuAr lamp exposures obtained after each exposure of Star A. The wavelength calibration has an rms of 0.05 Å and the spectra have a resolution of 3.9 Å FWHM based on CuAr lines. Individual spectral exposures were reduced using standard flat fielding and wavelength rectification procedures before being transformed to the Local Standard of Rest (LSR) velocity frame and combined.

¹As of this writing, the SIMBAD database lists it as a galaxy, presumably on the basis of its infrared colors, which include some star-forming galaxies.

We also obtained single 5–10 s exposures of 22 bright B-type dwarfs and giants from the Smithsonian Astrophysical Observatory Star Catalog for use in calibrating the spectral type of Star A. The spectra were reduced and calibrated in the same manner as described above. Table 1 lists these stars along with equivalent width measurements for prominent H and He lines. These spectra have typical signal-to-noise ratios (S/N) exceeding 200:1 in the middle of the spectral range observed.

3. Analysis

3.1. Optical Spectra and Spectral Type of Star A

Figure 2 shows the average spectrum of Star A between 5300 Å and 6600 Å. The peak signal-to-noise ratio near the middle of the spectrum is 65:1, but it is significantly lower toward the blue end beyond the pictured range. Labels denote key spectral diagnostic lines including He II $\lambda 5411$ (not detected), and the detected lines of He I $\lambda 5876$ and H α . H β and H γ are also detected but not labeled owing to poorer S/N. All other spectral features are interstellar, including several diffuse interstellar band features (DIB; Jenniskens & Désert 1994) and the Na I doublet, $\lambda\lambda 5889, 5895$. The presence of He I $\lambda 5876$ indicates a relatively hot star, while the apparent absence of He II $\lambda 5411$ means that Star A is not among the hottest O stars and is B0.5 or later (Kerton et al. 1999).

We used the robust curve fitting package MPFIT (Markwardt 2009) in IDL to measure equivalent widths and uncertainties for the He II $\lambda 5411$, He I $\lambda 5876$, and H α lines in this portion of the spectrum. Initially line positions, widths, and depths were allowed to vary as free parameters. He II $\lambda 5411$ is not detected, so we measured an upper limit by fixing the width of this line to the value computed for the $\lambda 5876$ line and constraining the position to lie within 1 Angstrom (55 km s^{-1}) of the rest wavelength. Table 1 gives the measured He and H line EWs and uncertainties for Star A. No emission lines were detected either at the location of the star or at locations along the slit covering the bowshock nebula.

The red spectral range covered in our data is not one commonly employed for spectral typing of hot stars owing to the paucity of spectral features. Consequently, we developed a series of diagnostic diagrams using the EW of He and H lines to measure the spectral type of Star A more precisely. Figure 3 shows the ratio of He II $\lambda 5411$ equivalent width to that of He I $\lambda 5876$ as a function of temperature/spectral type. Crosses, asterisks, and pluses denote early type stars from our measurements of spectra in the Jacoby et al. (1984) spectral atlas for luminosity classes I, III, V, respectively. The upper ordinate gives the spectral type of these stars. Open squares and triangles mark the measurements of Tlusty (Lanz & Hubeny

2003; Hubeny & Lanz 1995) model atmospheres with solar metallicity and temperatures as given on the lower ordinate. We adopt the relation between spectral type/luminosity class and effective temperature/surface gravity provided by Martins et al. (2005) in order to ensure consistency between the upper and lower ordinates. The atlas O star dwarfs (pluses) and model O star atmosphere dwarfs (triangles) show good agreement. A dashed line marks a third-order polynomial fit to the pluses and asterisks, and this expression is given near the top of the plot, where t_3 is stellar effective temperature in thousands K. Evolved stars and models with lower surface gravity characteristic of evolved stars lie systematically above this line.

Star A has a ratio $\text{EW}(\text{He II } \lambda 5411)/\text{EW}(\text{He I } \lambda 5876) < 0.14$, making it cooler than any star on Figure 3, and therefore, later than B0. We constructed two additional diagnostic diagrams appropriate for cooler, B-type stars, using the line measurements from SAO stars in Table 1, supplemented with a few additional early B star spectra from the Cygnus OB2 radial velocity survey of Kiminki et al. (2007, 2009). He and H line EWs were measured in the same way using the MPFIT code within IDL. Figure 4 plots the $\text{EW}(\text{He I } \lambda 5876)$ versus temperature/spectral type (*upper panel*) and the ratio $\text{EW}(\text{H}\alpha)/\text{EW}(\text{He I } \lambda 5876)$ versus temperature/spectral type (*lower panel*). As in Figure 3, pluses denote dwarfs (Lum. V), asterisks denote giants (Lum. III), and triangles denote Thursty (Lanz & Hubeny 2007) model atmospheres having $\log(g)=4.0$ appropriate to B dwarfs. Although the dispersion at any given spectral type is considerable, the data exhibit a well-defined monotonic trend. The solid line in each panel denotes the measurement for Star A, and dotted lines indicate the 1σ uncertainties. The dashed curve is a 3rd-order polynomial fit to all of the pluses and triangles. Analytic expressions for these curves appear within each panel, where t_3 is the temperature in thousands K. We match temperature to spectral type using the relations of Schmidt-Kaler (1982) which are very similar to the calibration of Underhill et al. (1979). While the measurements on real stars and model atmospheres compare favorably in the upper panel, the models are systematically displaced toward larger $\text{EW}(\text{H}\alpha)/\text{EW}(\text{He I } \lambda 5876)$ ratios in the lower panel. We believe that this is the result of broad Balmer wings which are measurable in the model $\text{H}\alpha$ lines but not in the lower S/N data. Interestingly, the giants and dwarfs show good agreement in both panels.

Figure 4 shows that the spectral type of Star A is near B0.5 on the basis the $\text{EW}(\text{He I } \lambda 5876)$ measurement (*upper panel*) and nearer B3 on the basis of the $\text{EW}(\text{H}\alpha)/\text{EW}(\text{He I } \lambda 5876)$ measurement (*lower panel*). Unfortunately, there are few spectral diagnostics sensitive to temperature for early B stars in the spectral range available. Traditional spectral type diagnostics in the blue end of the optical regime are not helpful in our spectra because of low S/N—a consequence of reduced instrumental sensitivity and high interstellar reddening which suppresses the blue flux from Star A. We adopt a spectral type of $\text{B1.5} \pm 1.0$. H or He

emission lines, often seen in B supergiants, are not evident in our spectrum of Star A. Furthermore, the $H\alpha$ and $H\beta$ linewidths in star A are 15–18 Å FWHM—more typical of dwarfs and much broader than the Balmer lines in any of our comparison B giants. Therefore, we adopt a luminosity of class of V.

3.2. Star A Spectral Energy Distribution and Distance

Table 2 lists eight optical and infrared photometric measurements for Star A compiled from available databases. These include the B2, R2, I2 entries from the USNO-B1.0 catalog (Monet et al. 2003), the JHK entries from the 2MASS Catalog, and *SST* [3.6] and [4.5] data from the GLIMPSE Point Source Catalog. Magnitudes have been converted to Jy using standard zero points available in the respective documentation. The optical data points are particularly uncertain, as they come from photographic surveys, so we adopt uncertainties of 15%. The infrared photometry from 2MASS and GLIMPSE has uncertainties of 0.03 mag, or about 3%. The red colors in any two bandpasses suggest a high degree of reddening for an early B star which has close to zero intrinsic color.

Figure 5 shows the optical and infrared spectral energy distribution of Star A. The solid curve is a blackbody approximation to a B1.5 V star with temperature $T=23,000$ K, radius $R=6.1 R_{\odot}$ (interpolated from Drilling & Landolt 2000), and $A_V=5.6$ mag of reddening according to a Cardelli et al. (1989) extinction curve in the optical and near-infrared and an Indebetouw et al. (2007) reddening law in the mid-infrared. The data are well fit by the model for a distance of ~ 4.0 kpc. The fit is quite good in the infrared where the photometry is most accurate and less good in the optical regime where photometric uncertainties are considerable. Nevertheless, the SED constrains the extinction with within about $\Delta A_V \approx 0.4$. No infrared excess is apparent, as might be expected for evolved massive stars having free-free emission or stars hosting circumstellar material. This is consistent with our adoption of a dwarf (i.e., main sequence) luminosity class. Based on the fit in Figure 5, we adopt a distance of 4.0 ± 1 kpc to Star A and the bowshock nebula, where the uncertainty is dominated by the uncertainty of the star’s spectral type and intrinsic luminosity. At this distance $1''$ corresponds to 0.019 pc and the $\sim 2'$ angular diameter of the bowshock nebula corresponds to 2.3 pc. This also means that the $7''$ angular distance from Star A to the bowshock apsis translates to a linear distance of ≥ 0.13 pc, where the inequality accounts for the unknown inclination relative to the line of sight. Given that bowshock nebulae are most easily recognized when seen edge-on, the inclination is likely to be near 90° and the standoff distance, $R_0 \approx 0.13$ pc, similar to bowshocks from stars #2 and #5 in the Kobulnicky et al. (2010) study of Cygnus OB2.

3.3. Identification of ^{12}CO Molecular Complex

We examined the ^{12}CO velocity cube of the IRAS 03063+5735 region from the Canadian Galactic Plane Survey (Taylor et al. 2003). The data cube has velocity channels of width 0.81 km s^{-1} and a beamsize of $45'$ FWHM. There are three peaks of molecular emission along this sightline. Figure 6 shows the 1-dimensional ^{12}CO spectrum summed over the $2'$ square region surrounding IRAS 03063+5735. The first peak near 0 km s^{-1} covers this entire region out to $10'$ from the bowshock nebula with uniform surface brightness. This molecular component is likely to be affiliated with very local gas. The second component near $+5 \text{ km s}^{-1}$ appears as a small filament that crosses near the bowshock but bears no morphological resemblance to the diffuse ISM emission seen in the *SST* and *WISE* infrared images. The third component centered near -40 km s^{-1} shows a strong channel-by-channel morphological resemblance to the mid-IR PAH and hot dust emission. Figure 7 shows a color view of the extended IRAS 03063+5735 region with *SST* [3.6] and [4.5] in blue and green, respectively, and the *WISE* [22] in red. Contours show the ^{12}CO intensity integrated over the $-38 - -42 \text{ km s}^{-1}$ velocity channels. The ^{12}CO contours correspond to intensities of 5 through 35 K km s^{-1} in steps of 5 K, equivalent to H_2 column densities of 1.5 through $10.5 \times 10^{21} \text{ cm}^{-2}$ adopting a standard conversion factor of $\alpha = 3.0 \times 10^{20} \text{ cm}^{-2} (\text{K km s}^{-1})^{-1}$ (Solomon et al. 1987). Note that the location of the bowshock nebula coincides with a local maximum in the H_2 column density of approximately $4.5 \times 10^{21} \text{ cm}^{-2}$. If we estimate that this feature is a roughly spherical molecular cloud with radius $r = 1' \equiv 1.10 \text{ pc}$, then the implied number density is $N_{\text{H}_2} \simeq 600 \text{ cm}^{-3}$. We caution that this is only a gross average, as ^{12}CO is known to freeze out onto dust grains in the cold dense cloud interiors.

The similarity of the ^{12}CO and diffuse ISM morphology, along with the identification of a local ^{12}CO peak at the bowshock location, supports the association of the bowshock with the molecular complex. The radial velocity of Star A, which we measure to be $-59 \pm 18 \text{ km s}^{-1}$ by a Gaussian fit to the He I $\lambda 5876$ line, adopting a rest wavelength of 5875.6 \AA . This lends further support to the association of the bowshock with this particular molecular complex. In principle, one might expect a runaway star to show anomalously large velocities relative to the surrounding medium. However, given the clear bowshock morphology of the associated nebula, we would also expect such objects to have velocity vectors predominantly in the plane of the sky. Hence, the similarity between the radial velocity of Star A and the molecular cloud upon which it impinges is consistent with the observed geometry.

The Brand & Blitz (1993) rotation curve in the outer Galaxy shows that radial velocity is not a very precise distance indicator along this $\ell = 140^\circ$ sightline. Their Figure 2b shows gas at $\sim -40 \text{ km s}^{-1}$ associated with a wide range of distances from 2 to 6 kpc. Our spectrophotometric distance estimate to Star A of $4.0 \pm 1 \text{ kpc}$ links the molecular gas at

-40 km s^{-1} to a distance comfortably within that range.

3.4. IRAS 03063+5735 at other Wavelengths

IRAS 03063+5735 is not detected to a 3σ limit of 0.037 Jy in the CGPS 1420 MHz radio map of this region. Wouterloot et al. (1993) searched for but did not detect any OH or water masters from this infrared source.

As first demonstrated by Rubin (1968) the observed flux density of radio emission at frequency ν (F_ν) from an optically-thin, isothermal, H II region at a known distance can be related to the H-ionizing photon flux (Q) from the exciting OB star(s). In this study we will use values of Q tabulated from model atmospheres of OB stars to determine if an H II region surrounding an early B-type star should be visible in our radio continuum images.

Kerton et al. (1999) present a version of the Rubin (1968) formula for observations at 1420 MHz of an isothermal (7500 K) H II region containing only hydrogen. Using the stellar calibration of Crowther (2005) we find a B1.5 V star has $\log(Q) = 46.0$ which corresponds to $F_{1420} = 900d^2f$, where d is the distance in kpc and f is essentially a covering factor (ie., $f = 1$ would correspond to an ionization bounded region, $f = 0.25$ could apply to a blister-type region). For $f = 1$ and $d = 4$ we find $F_{1420} = 7 \text{ mJy}$. This corresponds to a source with $T_B = 1.1 \text{ K}$ in the CGPS ignoring any beam dilution. The average and standard deviation of brightness temperature of our 1420 MHz image in a 10×10 arcmin box surrounding the position of the bowshock is $T_B = 5.68 \pm 0.08 \text{ K}$ so the distance and spectral type are consistent with the non-detection of this object in the CGPS radio continuum images. The non-detection in the CGPS image actually puts a fairly strong limit on how early the star could be. For example, at O9 V $\log(Q) = 48.1$, and repeating the above calculation leads to $T_B = 139 \text{ K}$. Even with a very low value for f the H II region associated with a late O type star would be easily detectable. All of this is consistent with our non-detection of the He II $\lambda 4511$ line in the optical spectrum which shows that Star A is B0.5 V or later.

3.5. Bowshock SED

Figure 8 shows the (background-subtracted) spectral energy distribution of the nebula (asterisks) as measured in a large lima-bean shaped aperture in the *WISE* bandpasses at 3.6, 4.5, 12 and $22 \mu\text{m}$. The star is detected in the *WISE* W1 and W2 bands, so we have used the higher-resolution *SST* GLIMPSE photometry to subtract off the star’s contribution to the *WISE* W1 and W2 measurements. The diamonds and solid line show the data and

extincted blackbody fit for Star A alone. The dashed line shows a Draine & Li (2007) dust model fit by eye for a radiation field $u = 300$ times the average interstellar radiation field of $2.17 \times 10^{-2} \text{ erg s}^{-1} \text{ cm}^{-2}$ (Mathis et al. 1983), a PAH fractional contribution of 1.77% and a mean ISM number density of 600 cm^{-3} . The *WISE* W2 [4.5] datum lies well above the model, possibly because of a contribution from shocked molecular hydrogen in this band. The *IRAS* 60 and 100 μm data also show relatively poor agreement with the model, but the uncertainties on these data are large owing to the large ($4'$) beamsize and background subtraction complications. The diffuse infrared surface brightness varies substantially over the nebula, suggesting substantial spatial variations in the local dust and gas density. Variations in temperature and density throughout the nebula are certain to render the single averaged SED a gross oversimplification. Hence, the dotted line fit is mostly for illustrative purposes, especially given large uncertainties on the local number density in the vicinity of the bowshock.

3.6. Search for Associated Stellar Cluster

The apparent increase in stellar density just to the north-east of the Star A initially suggested the possibility of a stellar cluster at this location. However, a color-magnitude diagram using JHK photometry of 2MASS Catalog sources within a $1'$ radius shows that the stars have a considerable spread in color (hence, reddening), and no clustering in either color-color or color-magnitude diagrams is evident. Therefore, we find no evidence of a stellar cluster in this vicinity, at least to the depths probed by the 2MASS and GLIMPSE catalog data.

4. Discussion

4.1. Runaway or Low-Velocity Star?

The expected proper motion of an object at 4.0 kpc distance with a transverse motion of 30 km s^{-1} is $\sim 1 \text{ mas yr}^{-1}$, too small to have a measured proper motion even over decade time scales in multi-epoch photographic plate surveys. Indeed, the USNO-B1.0 Catalog does not report a proper motion. Hence, there is no direct evidence for Star A having a high space velocity. Rather, it is inferred as a possibility from the morphology of the nebula.

It is also possible that low-velocity stars moving in a medium with a density gradient (Wilkin 2000) can produce a bowshock-like nebula. The proximity of Star A to a molecular cloud having a maximum column density just ahead of the bowshock (see Figure 7) makes

this explanation worth considering. Perhaps Star A formed within or near the pictured molecular complex. However, formation of such a massive star typically requires relatively high column densities characteristic of massive molecular clouds and would be accompanied by the formation of other lower mass stars comprising a small embedded cluster. We find no evidence of either high column density molecular clouds (the highest is $10.5 \times 10^{21} \text{ cm}^{-2}$ at $85'' \equiv 1.6 \text{ pc}$ north of the bowshock) or a stellar cluster containing lower mass stars. Furthermore, the observed excess emission in the [4.5] band (Figure 8) would be well explained by emission from shocked H_2 if the nebula were a genuine shock. It is not clear whether a low-velocity B1.5 star carving a cavity within a local density gradient would generate a wind shock sufficient to produce excitation of H_2 . More detailed spectral information and shock modeling would be needed to determine if this is a possibility. Given the current data, we prefer the interpretation that Star A is encountering the molecular cloud for the first time after having traveled some distance from its point of formation at a high velocity.

4.2. Possible Origins of a Runaway Star

The orientation of the cometary bowshock nebula suggests that Star A’s direction of travel is roughly toward the equatorial north. We searched the SIMBAD database for young stars, star clusters, and H II regions up to 3 degrees to the south to identify candidate birthplaces of Star A. At a distance of 4.0 kpc and an assumed tangential velocity of 30 km s^{-1} (30 pc Myr^{-1}) in the plane of the sky, it would be reasonable to suppose that the star has traversed up to 600 pc (8° on the sky) or even more during its $\text{few} \times 10 \text{ Myr}$ main-sequence lifetime. However, given that the star is already below the Plane and moving toward Galactic north, adopting the maximum travel time allowed by the main-sequence lifetime implies a formation locale well outside the scale height of Milky Way molecular clouds required to form such a massive star. Therefore, we prefer the interpretation that the runaway has been ejected recently and confine our search within several degrees of its current location.

One likely candidate for Star A’s birthplace is the H II region and stellar cluster associated with IRAS 03064+5638 located 0.94° (64 pc) due south. Figure 9 shows a three-color image of the field around Star A with the CGPS 1420 MHz radio continuum in red, the *WISE* [11.1] in green, and the *WISE* [4.5] in blue. Contours indicated the ^{12}CO brightness of 5, 10, 15, 25, 30 K km s^{-1} integrated between LSR velocities of -31 and -43 km s^{-1} . The bright ridge of radio emission extending 2° north to south is a thermal radio filament at an unknown distance and powered by a yet-unidentified source (Green 1989). Both the bowshock nebula IRAS 03063+5735 and IRAS 03064+5638 have ^{12}CO peaks in this velocity range,

suggesting a common distance. IRAS 03064+5638 contains a stellar cluster characterized by Carpenter et al. (1993) as having a few mid-B type stellar members, for their adopted distance of 2.2 kpc. If located at 4.0 kpc instead, these become early B stars of comparable mass and age to Star A. The 1420 MHz radio flux of IRAS 03064+5638 is 101 ± 3 mJy, equivalent to a B0 V star at the adopted distance. Apparently, the IRAS 03064+5638 cluster contains at least one star more massive than Star A, making it an environment from which Star A could plausibly have been ejected. Three-body encounters which eject one star often result in the formation of a tight binary. Therefore, our working scenario predicts the existence of close early-B binary within IRAS 03064+5638. However, the extinction appears high at this location, and no suitably bright optical sources are visible.

The peak molecular column density at IRAS 03064+5638 is approximately $N(H_2)=4.5 \times 10^{21}$ cm $^{-2}$. The adjoining molecular clouds which lack bright IR emission have peak $N(H_2)$ almost twice this value, suggesting other possible sites of intermediate-mass star formation nearby. These, yet unidentified, sites of star formation could have also been the birthplace of star A.

Another possible origin for Star A is the open cluster NGC 1220, located a full 3° (~ 201 pc) to the south of Star A, but along the same vector pictured in Figure 9. Ortolani et al. (2002) identified 26 probable members of this open cluster, estimating a distance of 1800 ± 200 pc and an age of 60 Myr. While this denser and more populous cluster provides a suitable environment for ejecting a B star via N-body encounters, the much smaller heliocentric distance (if correct) makes a physical connection between NGC 1220 and IRAS 03063+5735/Star A less likely.

5. Conclusions

We have identified an *IRAS* infrared source IRAS 03063+5735, previously reported as a galaxy, to be a bowshock nebula powered an early B-type (B1.5 V) star. The infrared source was selected from among several hundred sources having *IRAS* color-color criteria matching those expected from soft UV radiation fields generated by intermediate-mass (i.e., B-type) stars. Our measurement of the -58 km s $^{-1}$ LSR radial velocity of the star, combined with ^{12}CO line maps, allow us to identify a molecular cloud complex at a common velocity and ~ 4.0 kpc distance. The bowshock is plausibly produced by the supersonic motion of a runaway B star as it impinges upon a local maximum in the molecular column density of $\sim 4.5 \times 10^{21}$ cm $^{-2}$. However, a low-velocity star within a local density gradient may also be capable of producing the observed phenomena. We identify the H II region and stellar cluster associated with IRAS 03064+5638 at a projected distance of 64 pc as one plausible birth

site for a runaway star. The association of a star having a spectrophotometric distance with a particular molecular feature adds another data point to help anchor the (poorly defined) rotation curve in the outer Galaxy.

We thank WIRO staff James Weger and Jerry Bucher for their indefatigable efforts that enable the Observatory to produce science. We thank Ed Churchwell, Bob Benjamin, and an anonymous referee for helpful suggestions. Grants from the National Science Foundation through AST-09-08239 and NASA through 09-ADP09-0097 enabled this work. This publication makes use of data products from the Wide-field Infrared Survey Explorer, which is a joint project of the University of California, Los Angeles, and the Jet Propulsion Laboratory/California Institute of Technology, funded by the National Aeronautics and Space Administration. This publication makes use of data products from the Two Micron All Sky Survey, which is a joint project of the University of Massachusetts and the Infrared Processing and Analysis Center/California Institute of Technology, funded by the National Aeronautics and Space Administration and the National Science Foundation. This research has made use of the SIMBAD database, operated at CDS, Strasbourg, France

Facilities: WIRO (), Spitzer () , WISE ()

REFERENCES

- Arvidsson, K., Kerton, C. R., Alexander, M. J., Kobulnicky, H. A., & Uzpen, B. 2010, *AJ*, 140, 462
- Blaauw, A. 1961, *Bull. Astron. Inst. Netherlands* 15, 265
- Brand, J., & Blitz, L. 1993, *A&A*, 275, 67
- Brown, D., & Bomans, D. J. 2005, *A&A*, 439, 183
- Carpenter, J. M., Snell, R. L., Schloerb, F. P., & Skrutskie, M. F. 1993, *ApJ*, 407, 657
- Cardelli, J. A., Clayton, G. C., & Mathis, J. S. 1989, *ApJ*, 345, 245
- Crowther, P. A. 2005, *Massive Star Birth: A Crossroads of Astrophysics*, 227, 389
- Cyganowski, C. J., Whitney, B. A., Holden, E., et al. 2008, *AJ*, 136, 2391
- Comerón, F. & Pasquali, A. 2007, *A&A*, 467, L23
- Conti, P. S., Leep, E. M., & Lorre, J. J. 1977, *ApJ*, 214, 759

- Davis, C. J., Kumar, M. S. N., Sandell, G., et al. 2007, MNRAS, 374, 29
- Draine, B. T., & Li, A. 2007, ApJ, 657, 810
- Drilling, J. S., & Landolt, A. U. 2000, in *Astrophysical Quantities*, ed. A. N. Cox (4th ed.; New York; Springer), 381
- Fazio, G. G., et al. 2004, ApJS, 154, 10
- Gies, D. R. 1987, ApJS, 64, 545
- Gies, D. R., & Bolton, C. T. 1986, ApJS, 61, 419
- Green, D. A. 1989, AJ, 98, 2210
- Gvaramadze, V. V. & Bomans, D. J. 2008, A&A, 485, L29
- Hubeny, I., & Lanz, T. 1995, ApJ, 439, 875
- Indebetouw, R., Robitaille, T. P., Whitney, B. A., Churchwell, E., Babler, B., Meade, M., Watson, C., & Wolfire, M. 2007, ApJ, 666, 321
- Jacoby, G. H. & Hunter, D. A. 1984, ApJS, 56, 257
- Jenniskens, P., & Désert, F. X. 1994, *Astronomy & Astrophysics Supplement Series*, 106, 39
- Kerton, C. R., Ballantyne, D. R., & Martin, P. G. 1999, AJ, 117, 2485
- Kerton, C. R. 2002, AJ, 124, 3449
- Kiminki, D. C., Kobulnicky, H. A., Kinemuchi, K., et al. 2007, ApJ, 664, 1102
- Kiminki, D. C., McSwain, M. V., & Kobulnicky, H. A. 2008, ApJ, 679, 1478
- Kiminki, D. C., Kobulnicky, H. A., Gilbert, I., Bird, S., & Chunev, G. 2009, AJ, 137, 4608
- Kobulnicky, H. A., Gilbert, I. J., & Kiminki, D. C. 2010, ApJ, 710, 549
- Lanz, T., & Hubeny, I. 2003, ApJS, 146, 417
- Lanz, T., & Hubeny, I. 2007, ApJS, 169, 83
- Markwardt, C. B. 2009, *Astronomical Data Analysis Software and Systems XVIII*, 411, 251
- Martins, F., Schaerer, D., & Hillier, D. J. 2005, A&A, 436, 1049
- Massey, P., & Thompson, A. B. 1991, AJ, 101, 1408

- Mathis, J. S., Mezger, P. G., & Panagia, N. 1983, *A&A*, 128, 212
- Monet, D. G., Levine, S. E., Canzian, B., et al. 2003, *AJ*, 125, 984
- Noriega-Crespo, A., van Buren, D., & Dgani, R. 1997, *AJ*, 113, 780
- Ortolani, S., Carraro, G., Covino, S., Bica, E., & Barbuy, B. 2002, *A&A*, 391, 179
- Povich, M. S., Benjamin, R. A., Whitney, B. A., Babler, B. L., Indebetouw, R., Meade, M. R., & Churchwell, E. 2008, *ApJ*, 689, 242
- Reach, W. T., Rho, J., Tappe, A., et al. 2006, *AJ*, 131, 1479
- Rubin, R. H., 1968, *ApJ*, 154, 391
- Schmidt-Kaler, T. 1982, in *Numerical Data and Functional Relationships in Science and Technology*, Vol. 2b, ed. K. Schaifers & H. H. Voigt (Berlin: Springer), 14
- Solomon, P. M., Rivolo, A. R., Barrett, J., & Yahil, A. 1987, *ApJ*, 319, 730
- Stone, R. C. 1982, *ApJ*, 261, 208
- Strutskie, R. M. et al. 2006, *ApJ*, 131, 1163
- Taylor, A. R., Gibson, S. J., Peracaula, M., et al. 2003, *AJ*, 125, 3145 & Churchwell, E. 1990, *ApJ*, 353, 570
- Underhill, A. B., Divan, L., Prevot-Burnichon, M.-L., & Doazan, V. 1979, *MNRAS*, 189, 601
- van Buren, D., & McCray, R. 1988, *ApJL*, 329, L93
- van Buren, D., Noriega-Crespo, A., & Dgani, R. 1995, *AJ*, 110, 2914
- Wilkin, F. P. 2000, *ApJ*, 532, 400
- Wouterloot, J. G. A., Brand, J., & Fiegle, K. 1993, *A&AS*, 98, 589
- Wright, E. L., Eisenhardt, P. R. M., Mainzer, A. K., et al. 2010, *AJ*, 140, 1868

Table 1. Star A and Comparison Star Line Measurements

Star	EW(HeII λ 5411) (\AA)	EW(HeI λ 5876) (\AA)	EW(H α) (\AA)	Spectral Type	Ref.
Star A	0.11 (0.10)	0.78 (0.11)	3.70 (0.71)	B1.5 V	1
DL Cam	0.24 (0.01)	1.03 (0.06)	2.20 (0.34)	B0 III	2
HD36822	0.13 (0.01)	0.84 (0.01)	2.52 (0.31)	B0 III	2
HD23180	<0.01	0.78 (0.03)	2.34 (0.43)	B1 III	2
HD30836	<0.01	0.80 (0.02)	2.17 (0.24)	B2 III	2
HD29248	<0.01	0.78 (0.02)	2.44 (0.31)	B2 III	2
HD31237	<0.01	0.81 (0.02)	2.28 (0.27)	B3 III	2
ϵ Cas	<0.01	0.52 (0.01)	3.37 (0.52)	B3 III	2
δ Per	<0.01	0.42 (0.01)	3.87 (0.51)	B5 III	2
λ Cet	<0.01	0.32 (0.01)	4.69 (0.68)	B6 III	2
HD16727	<0.01	0.22 (0.01)	4.79 (0.74)	B7 III	2
γ Per	<0.01	0.19 (0.01)	4.60 (0.65)	B8 III	2
MT378	<0.09	0.81 (0.05)	2.19 (0.14)	B0 V	3
MT429	0.13 (0.03)	0.69 (0.02)	2.43 (0.18)	B0 V	3
HD22951	0.02 (0.01)	0.71 (0.02)	2.59 (0.32)	B0.5 V	2
MT605	0.05 (0.02)	0.64 (0.02)	2.31 (0.15)	B1 V	3
MT365	0.05 (0.02)	0.72 (0.03)	2.43 (0.27)	B1 V	3
MT605	0.05 (0.02)	0.64 (0.02)	2.31 (0.15)	B1 V	3
MT187	0.03 (0.02)	0.67 (0.02)	2.39 (0.16)	B1 V	3
HD21856	<0.01	0.68 (0.02)	2.61 (0.33)	B1 V	2
HD24131	< 0.01	0.66 (0.01)	2.74 (0.36)	B1 V	2
HD11241	<0.01	0.81 (0.02)	2.95 (0.56)	B1.5 V	2
MT234	<0.01	0.67 (0.03)	2.90 (0.27)	B2 V	3
HD23990	<0.01	0.67 (0.01)	2.11 (0.41)	B2 V	2
MT298	<0.01	0.64 (0.07)	3.44 (0.54)	B3 V	3
29 Per	<0.01	0.60 (0.01)	3.82 (0.56)	B3 V	2
34 Per	<0.01	0.55 (0.01)	4.04 (0.63)	B3 V	2
53 Per	<0.01	0.58 (0.01)	3.83 (0.54)	B4 IV	2
31 Per	<0.01	0.58 (0.02)	3.77 (0.65)	B5 V	2
HD21278	<0.01	0.47 (0.01)	4.23 (0.63)	B5 V	2

Table 1—Continued

Star	EW(HeII λ 5411) (Å)	EW(HeI λ 5876) (Å)	EW(H α) (Å)	Spectral Type	Ref.
HD24504	<0.01	0.43 (0.02)	4.31 (0.76)	B6 V	2
HD18537	<0.01	0.23 (0.01)	4.84 (0.80)	B7 V	2
β Per	<0.01	0.23 (0.01)	4.30 (0.65)	B8 V	2

Note. — 1—This work; 2—SAO Star Catalog; 3—Massey & Thompson (1991); Kiminki et al. (2007)

Table 2. 2MASS 03101044+5747035 Photometry

Wavelength (μm)	Mag.	Flux (mJy)	Source
0.44	16.33	1.25	1
0.65	14.54	4.09	1
0.75	13.93	5.68	1
1.2	12.04	26.2	2
1.6	11.38	28.4	2
2.2	11.03	24.0	2
3.6	10.82	13.8	3
4.5	10.78	9.19	3

Note. — 1–The USNO-B1.0 Catalog, (Monet et al. 2003); 2–2MASS (The Two Micron All Sky Survey 2006); 3–GLIMPSE 360 Point Source Catalog

Table 3. IRAS 03063+5735 Photometry

Wavelength (μm)	Flux (Jy)	Notes
W1 3.6	0.21	1
W2 4.5	0.23	1
W3 12.1	4.6	1
W4 22.0	4.9	1
IRAS 60	33.7	2
IRAS100	83.8	2

Note. — We adopt a 10% uncertainty on the flux measurements at all *WISE* bandpasses and a factor of 2 for the two *IRAS* measurements. 1—The reported flux reflects the entire nebula in a large aperture minus the flux from the star, as measured from *SST* GLIMPSE photometry, as reported in Table 2; 2—*IRAS* Point Source Catalog value. The *IRAS* measurements at 12 and 25 μm are systematically a factor of about 1.8 lower than the W3,W4 *WISE* measurements in similar bandpasses. This discrepancy probably reflects the much larger *IRAS* beam-size and associated uncer-

tainty in subtracting the diffuse background emission.

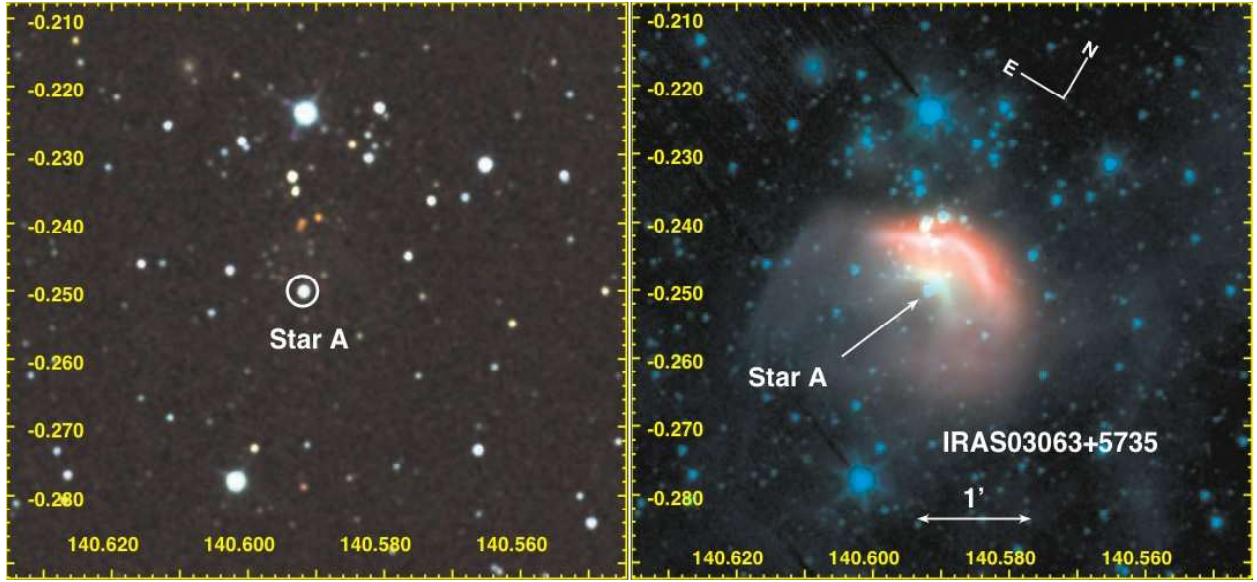


Fig. 1.— (right panel) *SST* three-color image in Galactic coordinates of the IRAS 03063+5735 region with *SST* [3.6] in blue, [4.5] in green, and *WISE* W3 $12\ \mu\text{m}$ in red, revealing the double bowshock morphology of the nebula. (left panel) 2MASS J/H/K image of the same field in blue/green/red, respectively. The star 2MASS03101044+5747035 (Star A) lies at the center of the nebula and can be seen in both images.

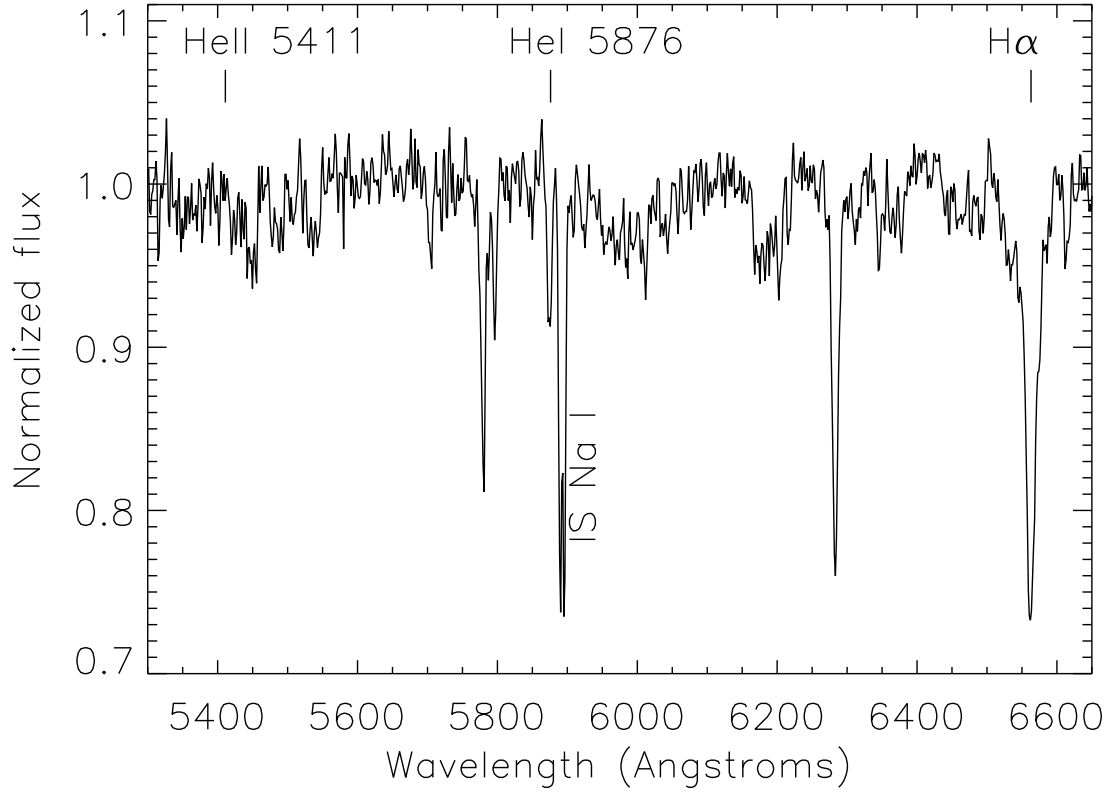


Fig. 2.— Averaged WIRO spectrum of 2MASS03101044+5747035. Locations of stellar He II $\lambda 5411$ (not detected), He I $\lambda 5876$ and H α are marked. Other absorption lines are interstellar, including Na I $\lambda\lambda 5889, 5895$ and several diffuse interstellar band features.

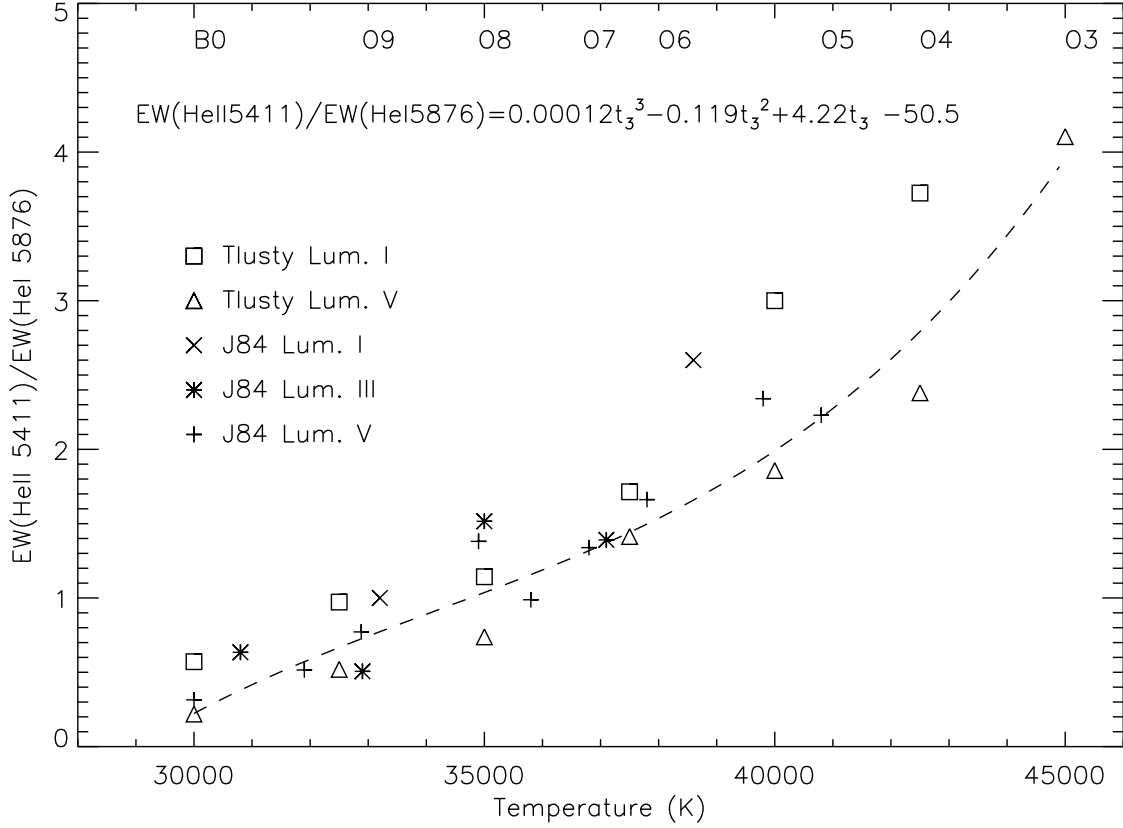


Fig. 3.— Ratio of He II $\lambda 5411$ equivalent width to He I $\lambda 5876$ EW versus spectral class/temperature for early type stars from the Jacoby et al. (1984, J84) spectral atlas (upper ordinate) and the Trusty (Lanz & Hubeny 2003) model atmospheres (lower ordinate), for both luminosity class V (dwarf) and III (giant) stars, as indicated by the legend. The dashed line shows the third-order polynomial fit to the luminosity class V models and spectral atlas stars, as described by the equation. Star A has a ratio $\text{EW}(\text{HeII } \lambda 5411)/\text{EW}(\text{HeI } \lambda 5876) < 0.14$, indicating a spectral type later than B0.

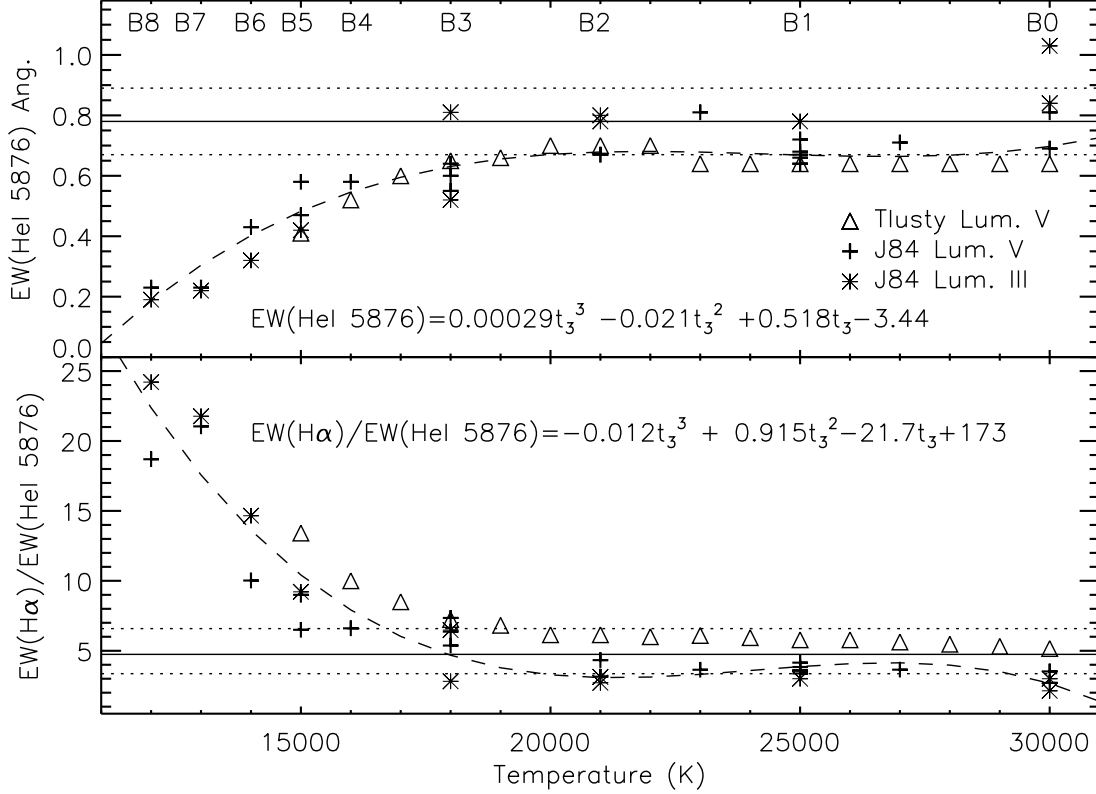


Fig. 4.— (*upper panel*) EW of He I $\lambda 5876$ versus temperature/spectral type for B type stars. (*lower panel*) Ratio of H α to He I $\lambda 5876$ equivalent width versus temperature/spectral type. Pluses denotes dwarfs (Lum. V) from Table 1 while asterisks denote giants (Lum. III). Triangles are model atmospheres from Lanz & Hubeny (2007). The dashed curve shows a 3rd-order polynomial fit to the pluses and asterisks. The solid line and dotted lines show the measurements and 1σ uncertainties for Star A.

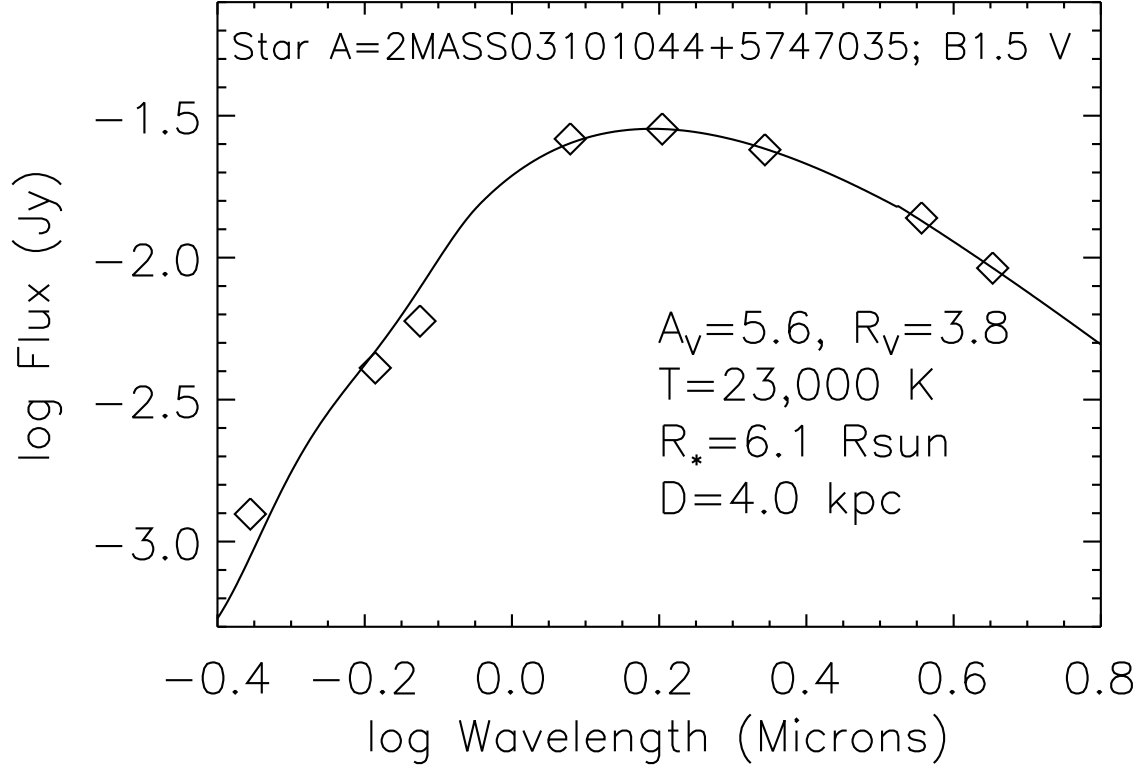


Fig. 5.— Spectral energy distribution for Star A. The curve is a blackbody with $T=23,000\text{K}$ and radius $R=6.1 R_{\odot}$ appropriate for a B1.5 V star, interpolated from the data of Drilling & Landolt (2000), with $A_V = 5.4$ mag and a Cardelli et al. (1989) extinction law in the optical and Indebetouw et al. (2007) extinction law in the mid-IR. A distance of 4.0 kpc yields a good fit.

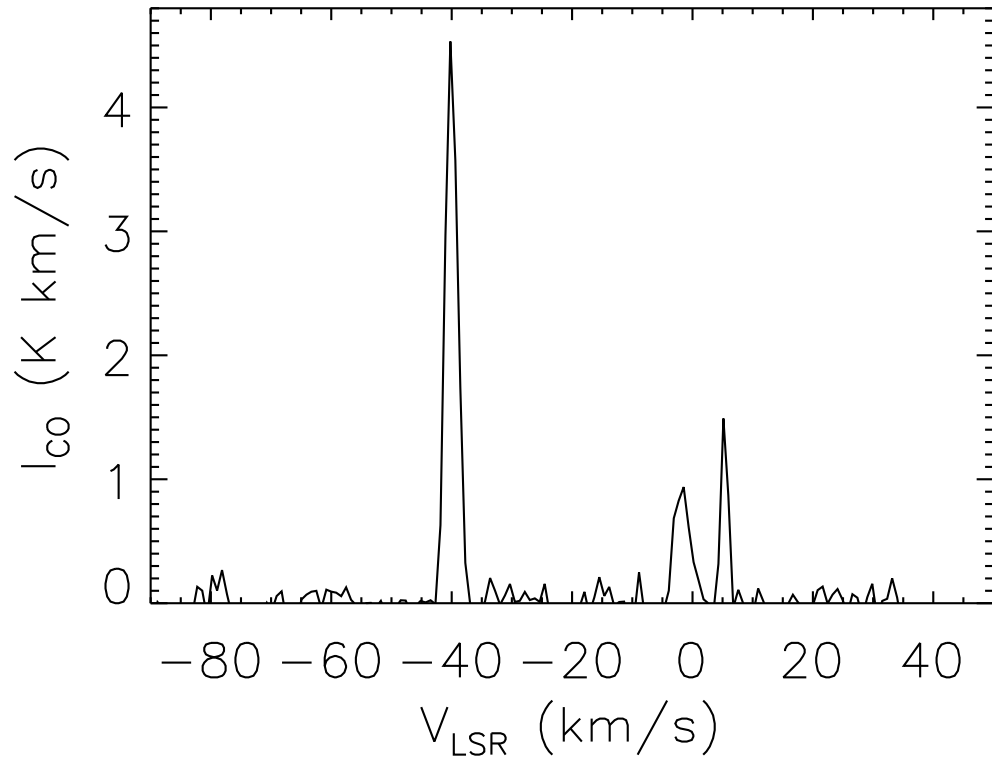


Fig. 6.— A 1-dimensional ^{12}CO spectrum from the CGPS along the IRAS 03063+5735 sightline averaged over a square $2'$ region. The molecular component near -40 km s^{-1} bears a strong morphological similarity to the diffuse emission from warm dust.

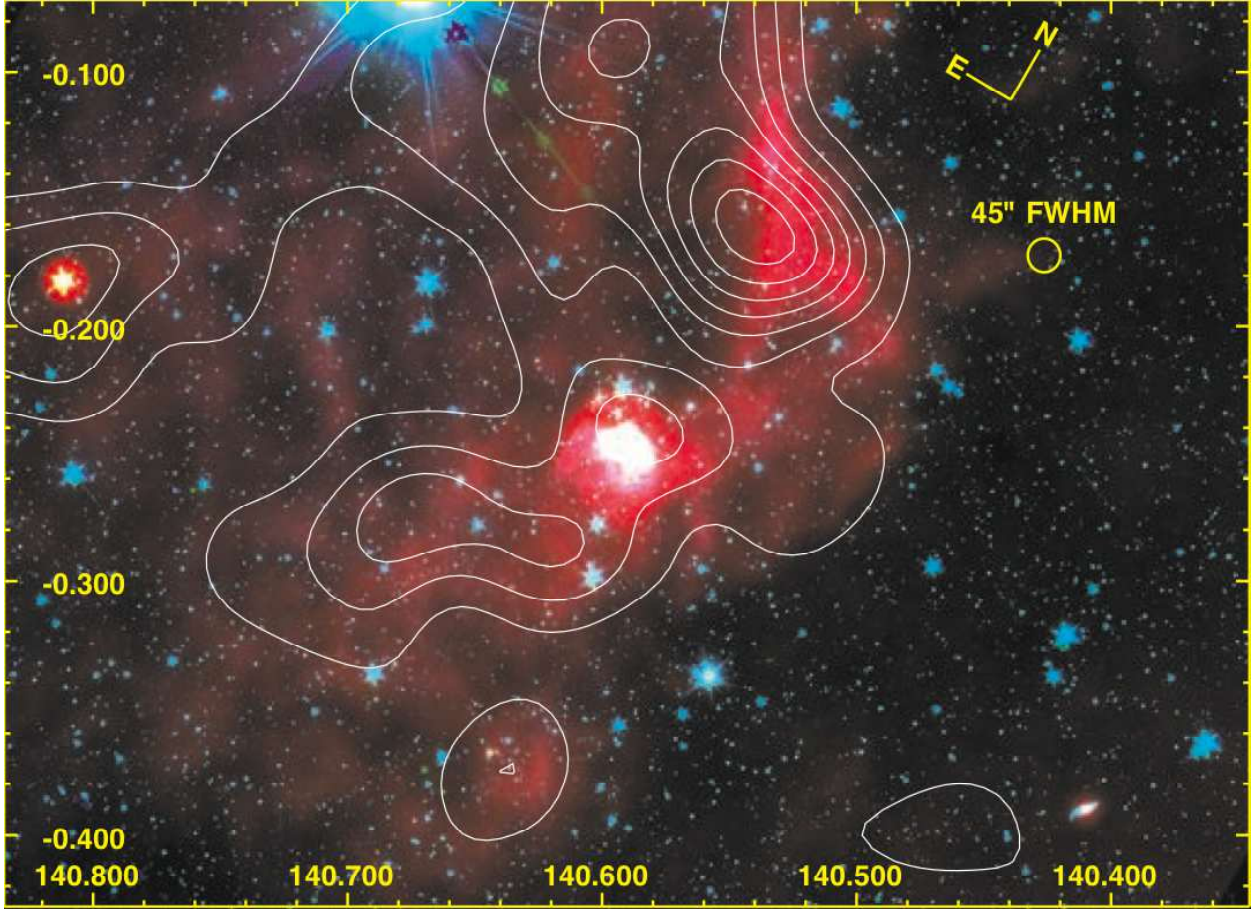


Fig. 7.— A color representation of the larger IRAS 03063+5735 region in Galactic coordinates with *SST* GLIMPSE [3.6] in blue, [4.5] in green, and the *WISE* [22] in red. Contours show the ^{12}CO brightness map from the CGPS integrated over the LSR velocity range -38 to -42 km s $^{-1}$. The ^{12}CO contours correspond to H_2 column densities of $1.5 \times 10^{21} \text{ cm}^{-2}$ – $10.5 \times 10^{21} \text{ cm}^{-2}$ in steps of $1.5 \times 10^{21} \text{ cm}^{-2}$.

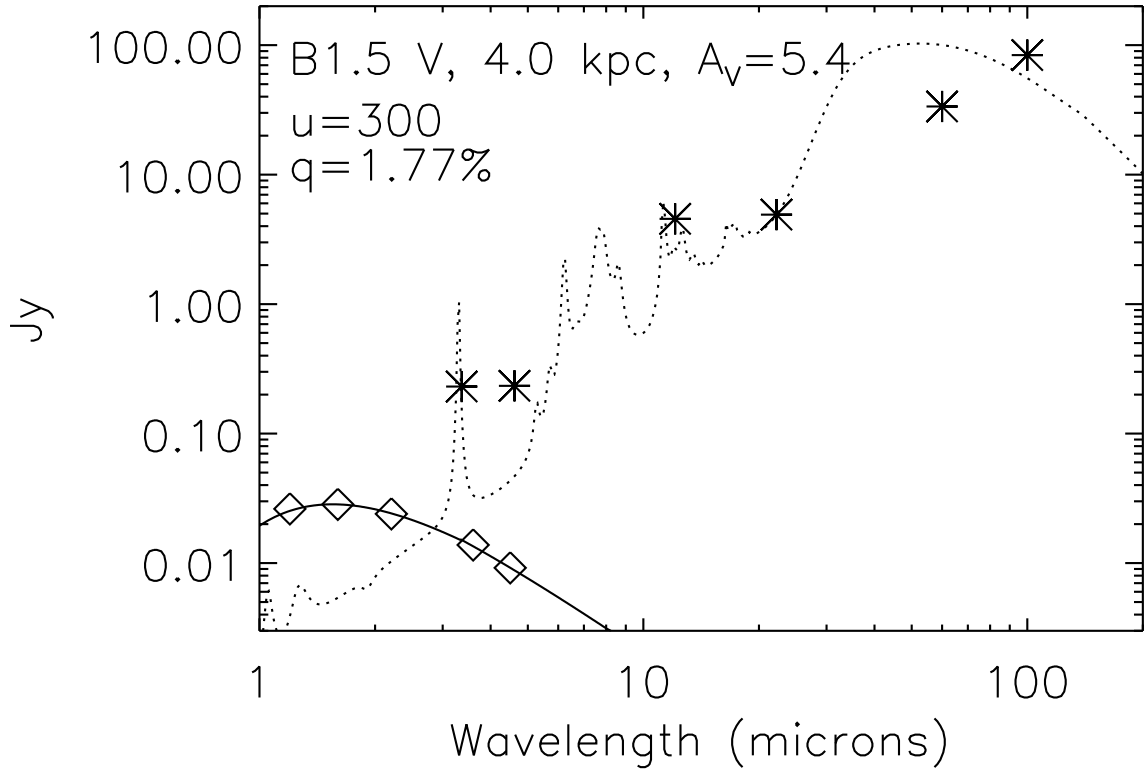


Fig. 8.— The spectral energy distribution of the IRAS 03063+5735 bowshock nebula (asterisks) from the four *WISE* bandpasses and two *IRAS* measurements at 60 and 100 μm . Diamonds and the solid line show the extinguished stellar SED. The dotted line shows a Draine & Li (2007) dust model with radiation intensity $u = 300$ times the mean interstellar radiation field (Mathis et al. 1983) and PAH contribution 1.77%.

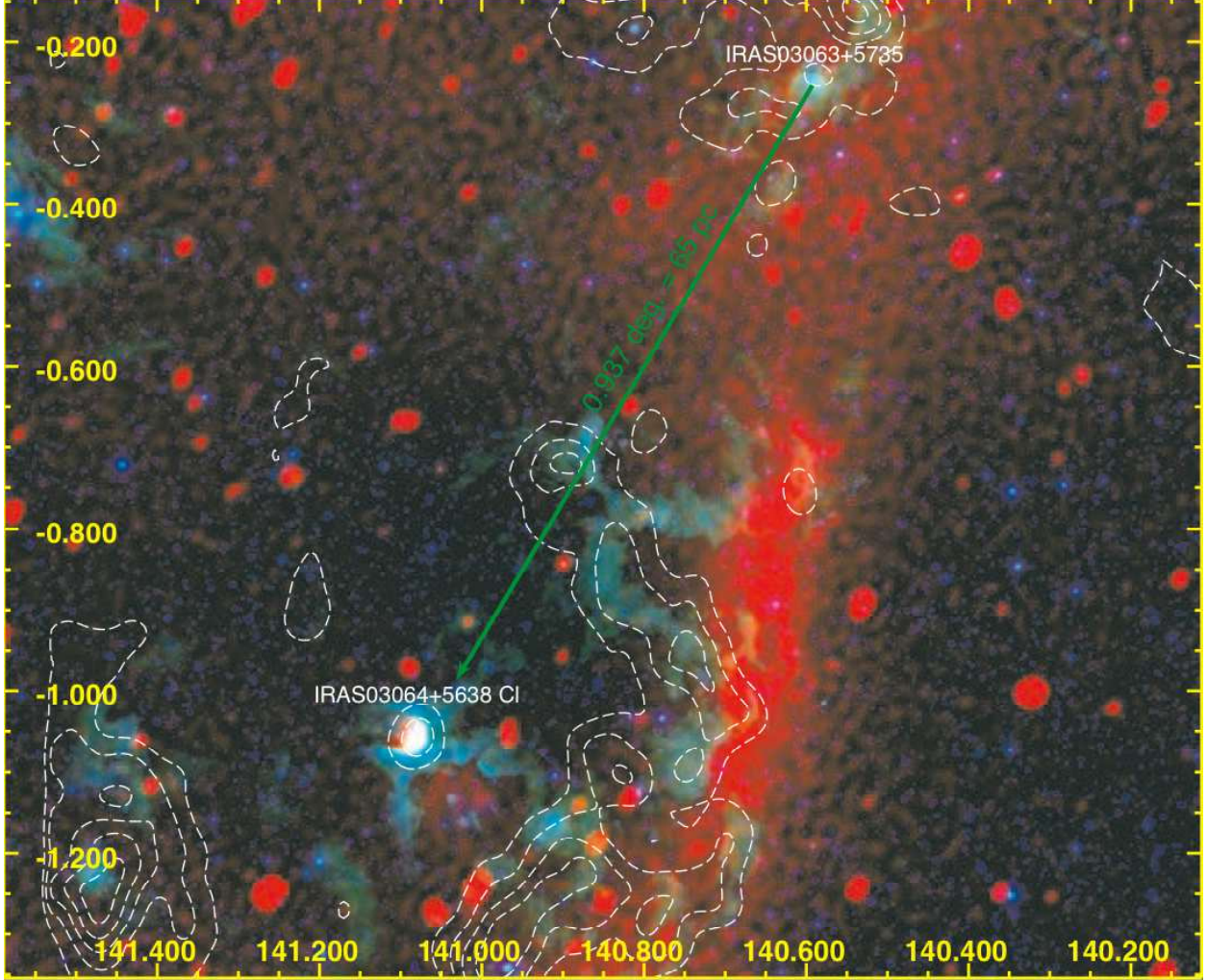


Fig. 9.— Color representation of the field around IRAS 03063+5735 as seen in the 1420 MHz CGPS radio continuum map (red), *WISE* W3 [11.1] (green), and *WISE* W2 [4.5] (blue). Contours depict the ¹²CO integrated between LSR velocities of -31 km s⁻¹ and -43 km s⁻¹. A green arrow points rearward along the bowshock axis of symmetry to a hypothetical birthplace of Star A near the H II region and stellar cluster associated with IRAS 03064+5638 at a projected distance of 65 pc.